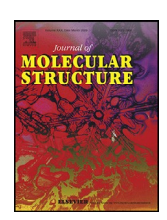
ELSEVIER

Contents lists available at ScienceDirect

# Journal of Molecular Structure

journal homepage: www.elsevier.com/locate/molstr



Supramolecular Co(II) complexes based on dithiolate and dicarboxylate ligands: Crystal structures, theoretical studies, magnetic properties, and catalytic activity studies in photocatalytic hydrogen evolution



Suman Adhikari <sup>a,\*</sup>, Afzal Hussain Sheikh <sup>b</sup>, Sevgi Kansız<sup>c</sup>, Necmi Dege<sup>d</sup>, Nabajyoti Baildya <sup>e</sup>, Ghodrat Mahmoudi <sup>f,g,\*\*</sup>, Nurul Alam Choudhury <sup>b</sup>, Raymond J. Butcher <sup>h</sup>, Werner Kaminsky <sup>i</sup>, Savannah Talledo <sup>j</sup>, Eric M. Lopato <sup>j</sup>, Stefan Bernhard <sup>j</sup>, Julia Kłak <sup>k,\*</sup>

- <sup>a</sup> Department of Chemistry, Govt. Degree College, Dharmanagar, Tripura(N) 799253, India
- <sup>b</sup> Department of Chemistry, Nagaland University, Lumami, Nagaland 798627, India
- <sup>c</sup> Faculty of Engineering, Department of Fundamental Sciences, Samsun University, Samsun 55420, Turkey
- <sup>d</sup> Faculty of Arts and Sciences, Department of Physics, Ondokuz Mayıs University, Samsun 55139, Turkey
- <sup>e</sup> Department of Chemistry, Milki High School, Milki, Malda 732209, India
- f Department of Chemistry, Faculty of Science, University of Maragheh, P.O. Box 55181-83111, Maragheh, Iran
- <sup>9</sup> Molodogvardeyskaya Str 244, Samara State Technical University, Samara 443100, Russian Federation
- h Department of Inorganic and Structural Chemistry, Howard University, Washington DC 20059, United States
- Department of Chemistry, University of Washington, Seattle, WA 98195, United States
- Department of Chemistry, Carnegie Mellon University, 4400 Fifth Avenue, Pittsburgh, PA 15213, United States
- <sup>k</sup> Faculty of Chemistry, University of Wroclaw, Wroclaw 50383, Poland

## article info

Article history:
Received 8 December 2022
Revised 19 March 2023
Accepted 30 March 2023
Available online 4 April 2023

Keywords:
Supramolecular assemblies
Co(II)
Crystal structures
Hirshfeld surface analysis
Magnetic studies
Photocatalytic hydrogen evolution

#### abstract

Two supramolecular Co(II)-based coordination compounds have been harvested from dithiolate and dicarboxylate ligands. They have been structurally characterized by FT-IR, elemental analysis, and single crystal X-ray diffraction. Salt 1 consists of two ([tris (2-aminoethyl) amine Co] 1,1-dicyano-2,2ethylenedithiolate) + per thiosulphate ion linked through intermolecular hydrogen bonds. Compound 2, (pyridine-2,6-dicarboxylate)  $_2$ Co-5H $_2$ O-Co).2H $_2$ O, is stabilized by intramolecular O-H ···O hydrogen bonds. building ribbons that propagate along the [100] direction in the crystals. From HS analysis, it is observed that the major non-covalent interactions present in 1 are C-H ...O, N-H ...N, N-H ...S, and N-H ...O hydrogen bonds, which play an important role in stabilizing the crystal structure. In 2, out of all the noncovalent interactions, O···H/H···O interactions have major contributions to stabilize the crystal structure. Theoretical investigation on the molecular structures of the crystals also revealed that the major stabilizing factor for **1** is H-bonding along with  $\pi$ - $\pi$  stacking while that for **2** is co-ordinate bond between water and cobalt(II) ion. Direct current variable-temperature magnetic susceptibility measurements carried out on polycrystalline samples of 1 and 2 in the temperature range of 1.8-300 K shows the presence of magnetic anisotropy of the cobalt(II) ion in 1 and weak intermolecular exchange in 2. Further, both the compounds 1 and 2 are found to be highly efficient water reduction catalysts in terms of per Co turn-over-numbers at lower concentrations.

© 2023 Elsevier B.V. All rights reserved.

## 1. Introduction

Supramolecular assemblies fabricated from metal complexes containing dithiolate and dicarboxylate-based multifunctional lig-

ghodratmahmoudi@gmail.com (G. Mahmoudi), julia.klak@chem.uni.wroc.pl (J. Kłak) .

ands have advanced significantly during the past few decades owing to their exciting applications in magnetism, catalysis, material science, and biochemistry [1–3]. In view of the extremely high strengths of metal-sulfur as well as metal-oxygen bonds and their significant roles in a variety of biological processes, the research attention being devoted to metal complexes containing dithiolate and dicarboxylate-based multifunctional ligands remains exceptionally high. Such research efforts have received further momentum due to the natural ability of the functionalized dithiolate and dicarboxylate ligands to demonstrate adaptable coordina-

<sup>\*</sup> Corresponding authors.

<sup>&</sup>quot; Corresponding author at: Department of Chemistry, Faculty of Science, University of Maragheh, P.O. Box 55181-83111, Maragheh, Iran.

E-mail addresses: sumanadhi@gmail.com (S. Adhikari),

tion modes during complexation, thereby resulting in their utilization in constructing fascinating supramolecular frameworks. Structural chemistry of functionalized dithiolate and dicarboxylate ligands is astoundingly distinct and has a considerable edge over that of other organic ligands. Depending on the nature of metal ions, the dithiolate and dicarboxylate ligands can chelate and also bridge with various metal centers to create supramolecular architectures [4,5]. The coordination complexes comprising of dithiolate and dicarboxylate-based ligands have been extensively studied and the advancement of research work done in this field has been published in several research papers and review articles [6–18]. The catalytic activities, magnetic properties, and biological activities of metal complexes harvested from functionalized dithiolate and dicarboxylate-based ligands have stirred a lot of research interest in the arena of inorganic supramolecular chemistry [3,19,20].

Given the well-known importance of cobalt in molecular magnetism and catalysis, cobalt-based supramolecular assemblies, among all the transition-metal compounds, are particularly alluring due to their potential to influence the innovative fields of advanced functional materials [21-23]. Following the invention of single-molecule magnets (SMMs) based on lanthanide complexes, a number of complexes with 3d-series metals, such as Cr. Mn. Fe, Co, Ni, and Cu, have been investigated [24,25]. Cobalt(II) complexes have attracted a lot of research interest owing to their high magnetic anisotropy, a wide range of geometry and coordination numbers, robust first-order spin-orbit coupling, and non-integer ground spin state. The non-integer ground spin state may diminish the possibility of a quantum tunneling mechanism for the relaxation of the magnetization [26,27]. Despite significant advancements in Co(II)-based SMMs in recent years, it is still difficult to rationally develop desired magnetic materials based on cobalt complexes.

Due to its minimal adverse impact on environment, molecular hydrogen is one of the most efficient and cleanest renewable energy sources for the future [28]. A lot of research efforts have been devoted for understanding how to convert water to  $H_2$  using visible light and designing metal complexes for proton reduction. Many  $H_2$  evolution catalysts based on metal complexes have been discovered in recent years and thoroughly researched, particularly in non-aqueous media [29,30]. Over the past few years, extensive studies have been done on photocatalytic  $H_2$  evolution using cobalt-based catalysts [31–34].

Covalent interactions between donor atoms on ligands and metal ions dominate the primary coordination sphere but noncovalent contacts regulate the secondary coordination sphere. These bonding interactions affect many features of coordination compounds, including complex geometry, selectivity, and reactivity in metal-facilitated catalytic processes [34,35]. Non-covalent contacts, such as hydrogen bonding,  $\pi_-\pi$  stacking, cation  $\dots$ , anion  $\cdots \pi$ , C-H  $\cdots \pi$ , and other weak intermolecular contacts are crucial for the organization of structural units resulting in a wide range of fascinating catalytic and magnetic phenomena. The numerous non-covalent interactions identified in the metal complexes provide hope for a better understanding of the complicated processes that govern supramolecular frameworks as well as the reactivity/selectivity of chemical transformations [36-42] . A quantitative investigation of the diverse non-covalent contacts is, therefore, necessary to obtain an advanced knowledge of packing of the crystal. Single crystal X-ray analysis followed by computational studies related to structure-property relationships of the synthesised novel metal complexes is expected to provide a thorough understanding of the frail non-covalent contacts present in the crystal frameworks. The non-covalent contacts can be interrelated to their molecular functions and bonding patterns in metal complexes.

We are particularly interested in the dithiolate and dicarboxylate-based multifunctional ligands because of their ability to interact with a broad range of metals and produce complexes with vastly different binding constants. In addition, they can be functionalized rather easily, allowing them to be incorporated into desired architectures. While substantial progress has been made on multifunctional dithiolate and dicarboxylate-based ligands, the versatility of substituents on the ligand backbones are yet to be explored. The said exploration may lead to more complex supramolecular structures with interesting magnetic and catalytic properties.

Given these considerations and in the light of our general interest in exploring various dithiolate and dicarboxylate building blocks for the development of diverse functional metal compounds, the salient aims of the current work include: (i) expanding the usages of dithiolate and dicarboxylate ligands for the preparation of supramolecular Co(II) compounds, (ii) recognizing their structural and non-covalent interactions features, and (iii) examining their magnetic behavior and photocatalytic activity towards hydrogen generation.

### 2. Experimental

### 2.1. Materials and physical measurements

All chemicals were reagent grade, procured from commercial sources, and used without purification. The solvents were purified by standard procedures. The 1,1-dicyano-2,2-ethylenedithiolate dipotassium salt (K $_2$ *i-mnt*) was synthesized according to a procedure reported previously [43]. Fourier-Transform Infrared spectra were recorded on a Perkin-Elmer FT-IR spectrometer with KBr pellets in the range of 4000–400 cm $^{-1}$ . Elemental analysis was carried out in Perkin-Elmer 2500 Series II elemental analyzer. Cyclic voltammetry was performed on a CH-Instruments Electrochemical Analyzer-600C Potentiostat at a scan rate of 0.1 V s $^{-1}$  using negative scan polarity in a three-electrode system configuration.

## 2.2. Synthesis of the metal complex

To a stirred solution of  $Co(NO_3)_2$ - $6H_2O$  (1.03 mmol) in 20 mL of HPLC-grade methanol, a solution of tris (2-aminoethyl) amine (tetraen) ligand (3.09 mmol) dissolved in 15 mL of HPLC-grade methanol was added slowly with constant stirring at room temperature. After 30 mins of stirring,  $K_2^{i-mnt}$ .  $H_2O$  (1.03 mmol) ligand dissolved in 15 mL HPLC-grade methanol and sodium thiosulphate (1.03 mmol) dissolved in 10 mL of distilled water were slowly added to the reaction mixture, resulting in immediate formation of deep brown precipitate. The stirring was continued for 3 h. The compound was collected through filtration, washed a few times with methanol and ether, and dried. Single crystals of  $\bf 1$ , suitable for X-ray analysis were grown from a solution of Dimethyl Sulphoxide (DMSO).

Salt **1**: Yield: 72%,FTIR (n cm $^{-1}$ , KBr): 3428–3120 [n(N-H) symmetric and asymmetric stretching modes], 2930 (nC-H stretching), 2201 (nC=N stretching), 1612 (nN-H bending scissoring vibration), 1384 [n(C=C) absorption band], 1030 and 945 [n(=C $\S$ <sub>2</sub>) group], 899 and 889 [n(C-S) band],747 (nCo-S band), 521 and 479 (nCo-N band). *Anal*. Calc. for  $C_{20}H_{36}Co_{2}N_{12}S_{6}O_{3}$ : C, 29.92; H, 4.52; N, 20.94. Found: C, 29.90; H, 4.51; N, 20.92%.

Salt **2** was synthesized according to a previously described method [44].

Salt **2**: Yield: 68%,FTIR (n cm<sup>-1</sup>, KBr): 3480–3390 [n(O-H) symmetric and asymmetric stretching modes], 1616 (nC-O stretching), 1386 (n(C=C) absorption band), 592 (nCo-O band), 543 and 484

Table 1
Experimental details for crystal structures of 1 and 2.

Crystal Data	Complex 1	Complex 2
Chemical Formula	2(C <sub>10</sub> H <sub>18</sub> CoN <sub>6</sub> S <sub>2</sub> ) •O <sub>3</sub> S <sub>2</sub>	C <sub>14</sub> H <sub>16</sub> Co <sub>2</sub> N <sub>2</sub> O <sub>13</sub> •2(H <sub>2</sub> O)
Crystal system	Triclinic	Monoclinic
Space group	PĪ	P 2/ c
Temperature (K)	100 (2)	100 (2)
Formula weight (a.k.b.)	802.83	574.18
a, b, c ( Å)	16.1221 (6), 16.8450 (7), 17.3907 (8)	8.3476 (3), 27.1461 (8), 9.5826 (3)
α, β, γ (°)	63.710 (2), 69.397 (3), 59.872 (2)	90, 98.115 (1), 90
Crystal size (mm)	0.19 × 0.06 × 0.03	0.48 × 0.18 × 0.16
Volume, V ( Å <sup>3</sup> )	3610.9 (3)	2149.72 (12)
Calculated density (Mg/m 3)	1.477	1.774
F <sub>000</sub>	1656	1168
μ <sup>σος</sup> (mm <sup>-1</sup> )	1.31	1.62
Z `	4	4
Diffractometer	Bruker APEX-II CCD	Bruker APEX-II CCD
θ range (°)	$2.2 \le \theta_{\cdot} \le 26.0$	$2.3. \le \theta . \le 36.4$
Wavelength ( Å)	0.71073	0.71073
Measurement method	$\omega_{scan}$	$\omega_{scan}$
Absorption correction	Multi-scan	Multi-scan
$h_{\min}$ , $h_{\max}$	-19, 19	<del>-</del> 13, 10
$k_{\min}$ , $k_{\max}$	-20, 20	-45, 44
I <sub>min</sub> , I <sub>max</sub>	-21, 20	<b>–15</b> , <b>15</b>
T <sub>min</sub> , T <sub>max</sub>	0.471, 0.747	0.471, 0.747
R <sub>int</sub>	0.124	0.028
Reflections collected	25,499	34,360
Independent reflections	13,460	10,359
Observed reflections [ $I > 2$ $\sigma(I)$ ]	6084	9517
Refinement method	SHELXL18/3	SHELXL18/3
Parameters	775	355
$R[F^2 > 2 \sigma(F^2)]$	0.056	0.029
w R (F)	0.123	0.072
GooF = S	0.87	1.10
$\Box \rho_{\min}$ , $\Box \rho_{\max}$ (e/Å <sup>3</sup> )	-0.61, 0.63	-0.78, 0.74

(nCo-N band). Anal. Calc. for  $C_{14}H_{20}Co_2N_2O_{15}$ : C, 29.29; H, 3.51; N, 4.88. Found: C, 29.31; H, 3.50; N, 4.86%.

## 2.3. Crystallographic data collection and refinement

For recording the X-ray diffraction data for **1**, an inclusion free red prism was chosen, whereas a clear purple needle was chosen for **2**. The said data were collected with graphite-monochromatized Mo-K  $\alpha$  radiation ( $\lambda$  = 0.71073 Å) on a Bruker APEX-II CCD(100 (2) K) diffractometer [45]. The structures were solved using SHELXT [46], refinement was done using SHELXL-2018 with least-squares minimization versus  $F^2$  [47]. Multi-scan absorption correction was applied (SADABS)[48]. All H atoms were initially located in a difference Fourier map and were refined using a riding model. The H atoms were placed in geometrically idealized positions and constrained to ride on their parent atoms with C—H distances in the range 0.95–1.00 Å. The related experimental details for **1** and **2** are summarized in Table 1.

## 2.4. Hirshfeld surface analysis

Hirshfeld surface analysis [49] and fingerprint plots were generated with the *CrystalExplorer21* program [50] for investigating the different interactions in the crystal structures of **1** and **2**.

### 2.5. Theoretical studies

Ground-state geometry optimization of crystal systems **1** and **2** were performed with the help of Density Functional Theory using Gaussian 09 [51]. To determine the precise geometry of the crystals, B3LYPhybrid functional was used [52]. For the non-metal elements, 6–31G(d) basis function was used while for cobalt, the pseudopotential-based LANL2DZ basis set was employed.

### 2.6. Magnetic susceptibility measurements

A Quantum Design SQUID magnetometer (type MPMS-3) was used to assessmagnetic susceptibility and magnetization. Polycrystalline samples of  $\bf 1$  and  $\bf 2$  were subjected to direct current magnetic measurements in the temperature range of 1.8–300 K with an externally imposed magnetic field of 0.5 T. Corrections were made by subtracting the sample – holder signal and contribution  $\chi_{\rm D}$  estimated from the Pascal's constants [53] .

## 2.7. Photocatalytic hydrogen evolution

Compounds **1** and **2** were tested as water reduction catalysts (WRC) in a photocatalytic water reduction system using [Ir(Fmppy)  $_2$  dtbbpy]PF $_6$  (where Fmppy = 4 -fluoro-2-phenyl-5-methylpyridine, and dtbbpy = 4,4 -di-*tert* -butyl-2,2 -bipyridine) as the photosensitizer (PS), and triethanolamine (Alfa Aesar L04486) as the sacrificial donor (SD). Each test sample contained 750  $\mu$ L of a total solution comprising of 600  $\mu$ L of PS and WRC solutions in DMSO (J.T. Baker JT 9224) and 150  $\mu$ L of 30% w/w aqueous solution of SD. The reactions were conducted at a PS concentration range of 0.01 to 0.1 mM. Hydrogen evolution was measured on a parallel high-throughput photoreactor using colorimetric chemosensitive H $_2$  detector (DetecTape Hydrogen Detection Tape – Midsun Specialty Products, Item DT-H210015-PF4) as described previously [54,55].

### 3. Resultsand discussion

## 3.1. FT-IR spectral characterization

To comprehend the coordination modes of two ligands (tetraen and i-mnt 2-) to the Co(II) metal center, the FT-IR spectra of Co(II)

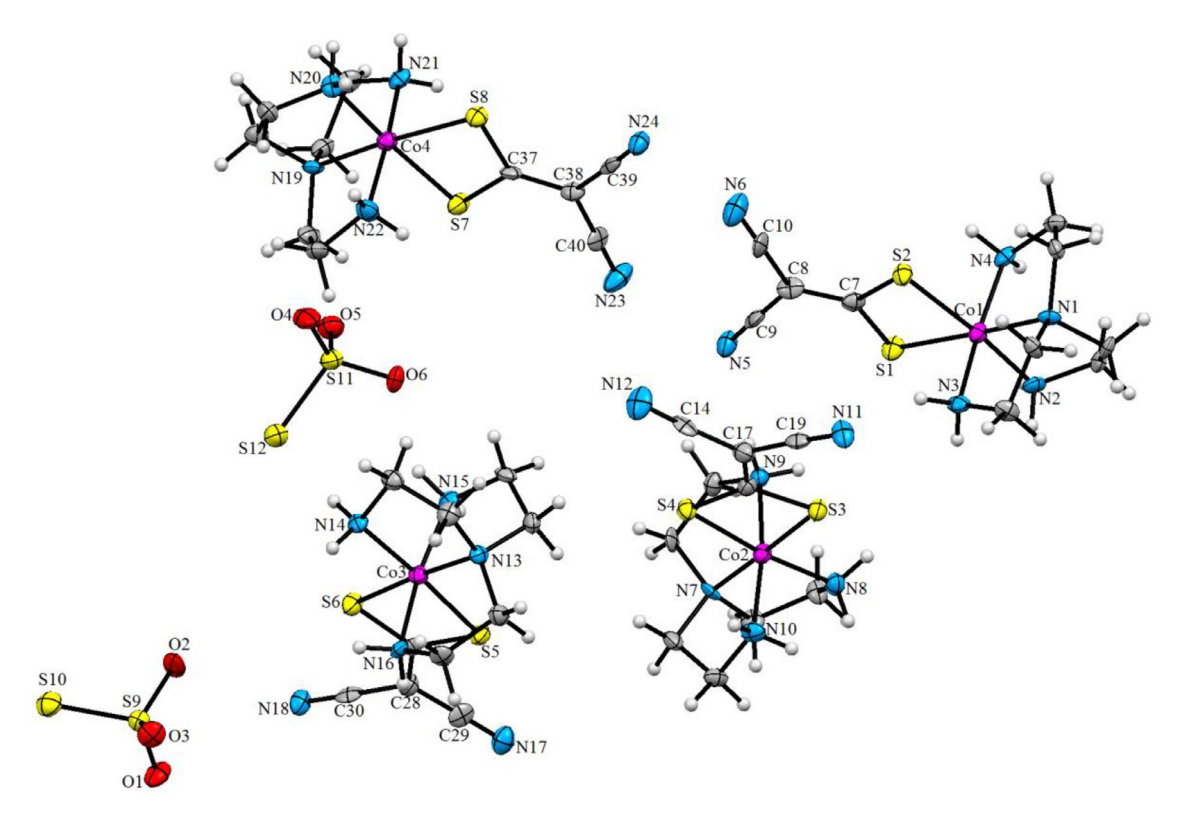


Fig. 1. The content of the asymmetric unit of 1. Thermal displacement ellipsoids are shown at their 50% probability levels.

complex 1 as well as those of the free ligands were thoroughly investigated. The pertinent data are shown in Figs. S1 and S2. The broad bands observed in the 3428-3120 cm<sup>-1</sup> region of the spectrum of  ${\bf 1}$  are ascribed to V(N-H) (asymmetric and symmetric) stretching modes of the amino nitrogen of tetraen ligand. The v(C-H) stretching band for **1** can be found at 2930 cm<sup>-1</sup>. The IR spectrum of 1 shows a strong absorption band at 2201 cm<sup>-1</sup>, which is attributed to the  $U(C \equiv N)$  stretching frequencies of the coordinated i-mnt 2- ligand. This confirms the formation of mixed ligand complex. The V(N-H) bending (scissoring) vibration for **1** is detected at 1612 cm<sup>-1</sup>, which is lower than that for free tetraen ligand (1636 cm<sup>-1</sup>). The observed shift to a lower frequency advocates that the amino nitrogen atoms of tetraen are coordinated to cobalt metal center. The stretching frequency of V(C=C) in 1 is observed at 1384 cm  $^{-1}$ , while the same for free ligand K $_2$  i-mnt is observed at 1365 cm  $^{-1}$ . The increased value of  $^{V}(C=C)$  stretching frequency indicates delocalization of  $\pi$  electrons, which also confirms the formation of the mixed ligand complex 1. Absorption bands at 1030 and 945 cm<sup>-1</sup> are due to =  $CS_2$  group. The V(C-S)band appearing at 870  ${\rm cm}^{-1}$  in the spectrum of free ligand i-mnt <sup>2-,</sup> appears at 899 and 889 cm<sup>-1</sup> in the spectrum of **1**, signifying symmetrical bonding of both the S atoms to the cobalt ion. The band at 747 cm<sup>-1</sup> is ascribed to Co-S vibration. The weak bands at 521 and 479 cm<sup>-1</sup> are ascribed to Co-N vibration.

### 3.2. Crystal structure description of complex 1

Fig. 1 depicts the asymmetric unit of **1**, which consists of two thiosulphate ions and four cobalt ions. The six coordinate Co1 center, existing in a distorted octahedral environment, is bonded to four enamine nitrogen (N1, N2, N3, and N4) of tris (2-aminoethyl) amine (*tetraen*) ligand and two sulfur atoms (S1 and S2) of *i-mnt*<sup>2-</sup> ligand. The coordination geometries of Co2, Co3, and Co4 ions are distorted octahedral, similar to that of Co1 center. The cobalt (II) ions and the two thiosulphate ion ligands are linked

to one another via intramolecular N3-H3 C···N11, N9-H9 A···N5, N14-H14 C··S12, N15-H15 D···O6, and C22-H22 B···O6 hydrogen bonds (Table S1). The molecules are linked by several intermolecular C-H ···O, C-H ···S, C-H ···N, N-H ···S, N-H ···N, and N-H ···O hydrogen bonds in the crystal structure, forming a 3D supramolecular framework (Figs. 2 and 3). The Co-S and Co-N bond distances are in 2.245-2.305 Å and 1.945-1.981 Å ranges, respectively. Compared to Co-S bonds, the Co-N bonds are shorter. Although, the Co-N bond distances are comparable with the same bond distances in reported cobalt compounds, the values reported herein are slightly shorter than the previously reported values [56.57]. While the shortest bond length, between two metal centers (Co1-Co2), is 6.948 Å, the longest distance is between Co1-Co4 with a value of 15.321 Å. The S1-Co1-S2, S3-Co2-S4, S5-Co3-S6, and S7-Co4-S8 bond angles have almost identical values (Table S2). Similarly, the N-Co-N bond angles are nearly identical. The bond angles around Co1 metal center, namely S1-Co1-S2, S1-Co1-N3, S2-Co1-N4, N1-Co1-N2, N1-Co1-N4, and N2-Co1-N3 are 76.88(6)°, 92.8(2)°, 88.5(2)°, 86.9(2)°, 85.0(2)°, and 90.4(2)°, respectively, which exhibit a distorted octahedral geometry. These prominent angle values are similarly observed around Co2, Co3, and Co4 metal centers. The S9-S10, S11-S12, S9-O1, S9-O2, S9-O3, S11-O4, S11-O5, and S11-O6 bond distances are 1.995(2), 2.023(2), 1.471(4), 1.469(4), 1.471(4), 1.480(4), 1.487(4), and 1.470(4) Å, respectively. These S-S and S-O bond lengths of thiosulphate ion are in good agreement and comparable with reported thiosulphate compounds [58,59].

## 3.3. Crystal structure description of complex 2

Despite the fact that the crystal structure of compound **2** has already been reported [44], we have chosen to gather the data once again to check for any substantial structural variations. Obviously, the structure is much the same, but there are a few differences that merit reporting. The molecular structure of **2** with pyridine-

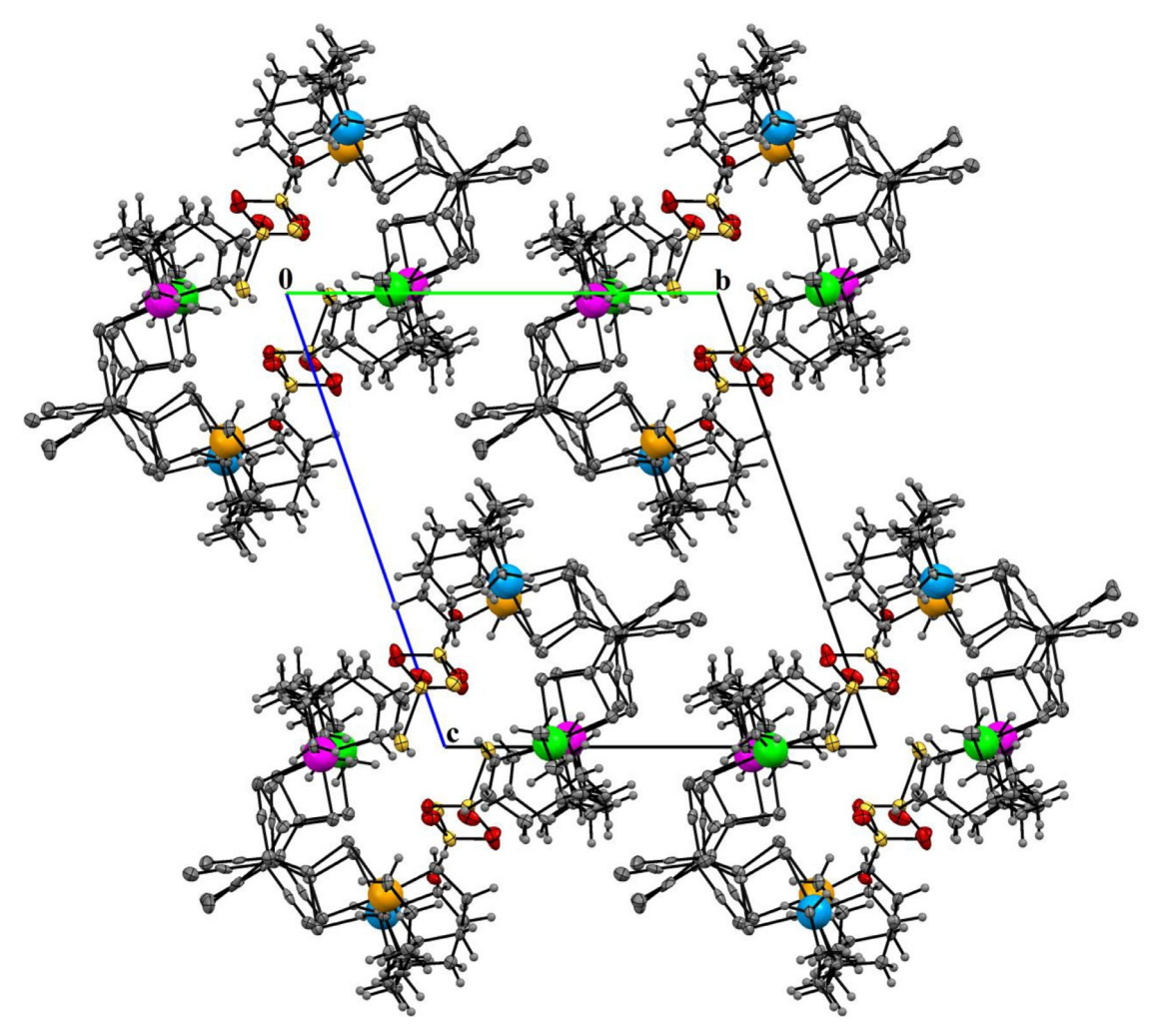


Fig. 2. A view of crystal packing of 1 along a -axis direction. (Co1: Purple, Co2: Yellow, Co3: Blue, and Co4: Green).

2,6-dicarboxylate or dipicolinate (dpc) is shown in Fig. 4. As shown in Fig. 4, the asymmetric unit of 2 contains one of the cobalt(II)cobalt(II) compounds [including  $Co(dpc)_2$ -O-Co-(H<sub>2</sub>O)<sub>5</sub>] and two additional water molecules. The Co1 ion has a distorted octahedral geometry with four oxygen and two nitrogen atoms from two dpc ligands, while the Co2 is octahedrally coordinated by five oxygen atoms of five water molecules and one oxygen atom of a carboxyl group. In **2**, the *dpc* acts as a tridentate ligand. The two cobalt(II) ions are linked to one another by the carboxyl groups, so the carboxyl group (O1-C1-O2) is in a bridging position. The complex is non-planar with two pyridine rings inclined to one another by making a dihedral angle of nearly 89.51(3)°. The cobalt(II)-cobalt(II) complex and two aqua molecules are linked to one another by intramolecular O5W-H5 W1···O1, O1W-H1 W1···O6W, and strong O4W-H4 W1...O7W hydrogen bonds. The molecules are linked by several intermolecular O-H ···O and C-H ···O type-hydrogen bonds in the crystal structure of 2, forming a 3D supramolecular framework (Fig. 5 and Table S3). In the previous study, as stated by Qi et al. [44], all water molecules inhere also participate in hydrogen bonding. Extensive intermolecular hydrogen bonds are formed in the crystal by means of the five coordinated water molecules (OW1, OW2, OW3, OW4, and OW5) and two crystal water molecules (OW6 and OW7). There are also weak  $\pi$ ... $\pi$  contacts between the two pyridine rings of  $dpc [Cg5\cdots Cg5^{i} = 3.724 (2) \text{ Å};$ here, C95 is center of the N1/C2-C6 ring and symmetry code (i); -x + 1, -y, -z + 1].

The Co-O dpc bonds are, on average, longer than the Co-O water bonds (Table S4). The Co-O bond distances vary from 2.0808(8) to 2.2117(8) Å with an average of 2.108 Å, which is comparable to that reported for Co(II) complexes [60]. In a previous study, Co-O distances were found in the range of 2.1160(19) to 2.2184(18) Å, and the average bond length was 2.1728 Å, which is consistent with the values here [44]. Co1-N1 and Co1-N2 bond distances are 2.0248(8) and 2.0207(9) Å, respectively, and the Co-N distances in the previous study were 2.015(2) and 2.022(2) A [44]. These lengths are close to 2.012(2) and 2.005(2) Å, as reported by Chkirate and co-workers [61]. C2-N1, C6-N1, C9-N2, and C13-N2 bond lengths are 1.3326(12), 1.3341(12), 1.3324(12), and 1.3300(12) Å, respectively. These C-N bond distances within pyridine rings are in good agreement with the corresponding bond lengths reported for pyridine compounds [62,63]. In the cobalt(II)-cobalt(II) complex, the carboxyl group distances are unremarkable with an average C-O bond distance of 1.258 Å, which is comparable to that reported for carboxylic compounds [64,65].

### 3.4. Hirshfeld surface analysis

Intermolecular interactions are important for crystal stability of crystalline compounds. Hirshfeld calculations have been frequently used in recent years to investigate different intermolecular interactions in the crystal structures [62,64,66–68]. The Hirshfeld surfaces were visualized with the 3D  $d_{\rm norm}$  mapped over fixed color scales of –0.410 to 2.782 Å (Molecule A), –0.392 to 2.271 Å (Molecule B),

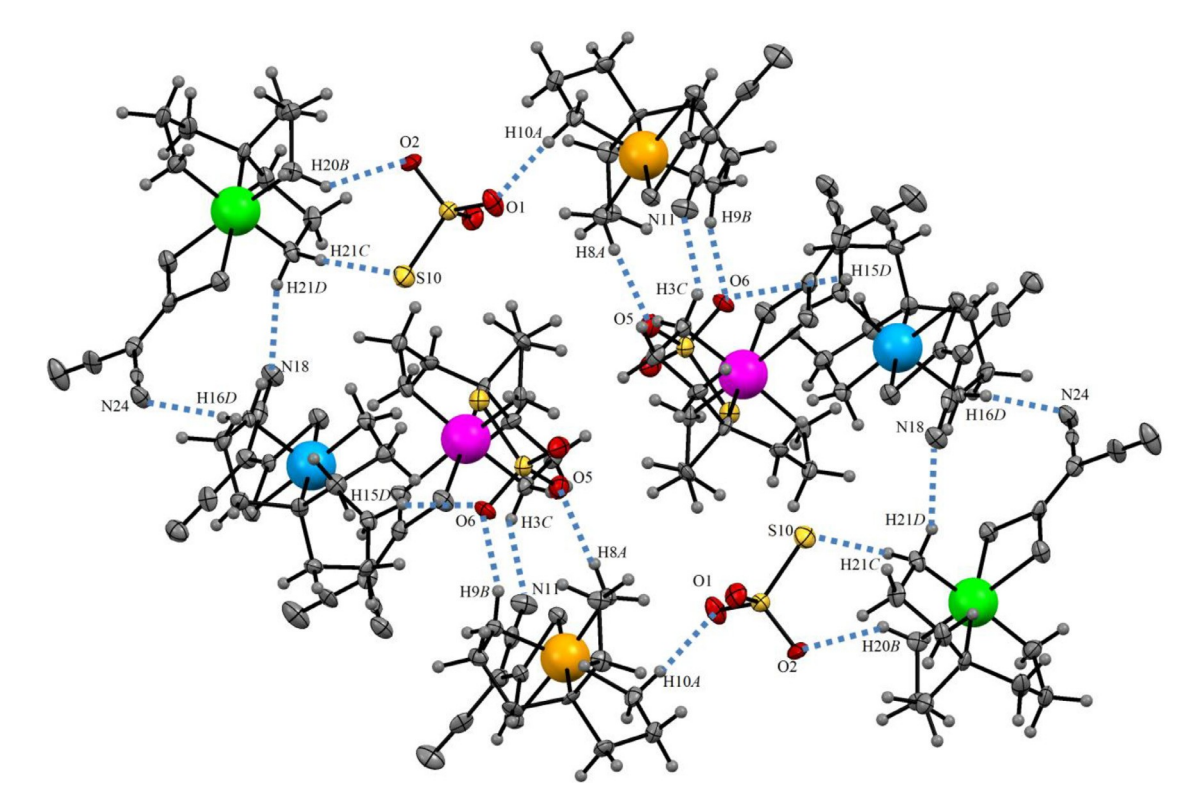
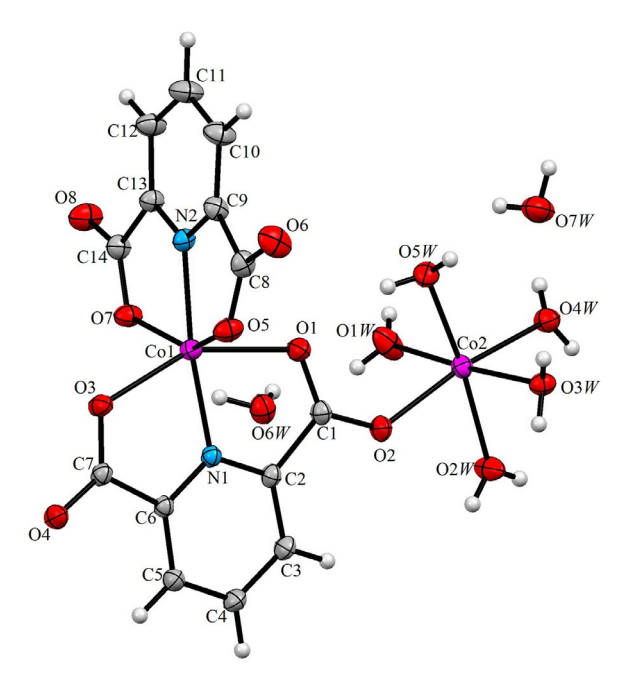


Fig. 3. A partial view of crystal packing of 1 showing hydrogen bonds. (Co1: Purple, Co2: Yellow, Co3: Blue, and Co4: Green).



**Fig. 4.** Molecular structure of complex **2** with the displacement ellipsoids drawn at 50% probability level.

-0.538 to 2.803 Å (Molecule C), and -0.491 to 2.785 Å (Molecule D) (Fig. 4). The red circles on the  $d_{\text{norm}}$  surface of molecules A, B, C, and D represent the C-H···O, N-H···N, N-H···S, and N-H···O interactions, respectively (Fig. 6). The major contacts of the compound are N···H (33%), H···H (22%), S···H (16%), and O···H (11%) for molecule A; N···H (34%), H···H (18%), S···H (16%), and O···H (12%) for molecule B; N···H (33%), H···H (29%), O···H (13%), and S···H (8%) for molecule C; and N···H (34%), H···H (31%), S···H (11%), and O···H

(6%) for molecule D (Fig. 7). The results show that the structure is stabilized by  $C-H\cdots O$ ,  $N-H\cdots N$ ,  $N-H\cdots S$ , and  $N-H\cdots O$  hydrogen bonds. Some other interactions that contribute to a lesser extent are also present.

In Fig. 8, the interactions are visualized by a 3D view of the molecular Hirshfeld surface mapped over  $d_{\text{norm}}$ ,  $d_{\text{i}}$ ,  $d_{\text{e}}$ , and shape index of the complex 2. On the  $d_{norm}$  Hirshfeld surface, bright red areas indicate H-bond interaction sites, represented by red dots (Fig. 9); the Hirshfeld surface mapped on  $d_{norm}$  range from 0.0783 to 1.0981 a.u. The red regions on the  $d_{\text{norm}}$  surface are located on the oxygen and hydrogen atoms, which contribute to non-covalent contacts, as established by the interactions in Fig. 8. The results of fingerprint analyses are given in Fig. 9. The interactions with a contribution of less than 1% are not included in the visualization. Fig. 10 summarizes the contributions of all the interactions. With a value of 49%, the contribution of O···H/H···O contacts has the largest share in the crystal packing of 2, wherein the heteronuclear contacts appear as spikes. The H···H contact has a smaller share with a contribution of 30% and C···H/H···C contacts with a contribution of 8%.

## 3.5. Magnetic susceptibility measurements

The ground state of high-spin octahedral Co(II) is  $^4T_{1g}$ . As the angular orbital momentum is largely quenched, it is difficult to interpret the magnetic moments of compounds with  $^7$  ground state terms that frequently exhibit significant temperature dependence [69–73]. These types of systems display significant zero field splitting, which results in considerable magnetic anisotropy because of the enormous spin-orbit coupling.

The magnetic characteristics of **1** were evaluated in the temperature range of 1.8–300 K. The magnetic susceptibility  $(X_mT)$  vs. Temperature plot (T) (where  $X_m$  is the molar magnetic susceptibility per Co(II) unit) is displayed in Fig. 11. The value of  $X_mT$  at room temperature is 2.50 cm<sup>3</sup>mol<sup>-1</sup> K, which is more than that antici-

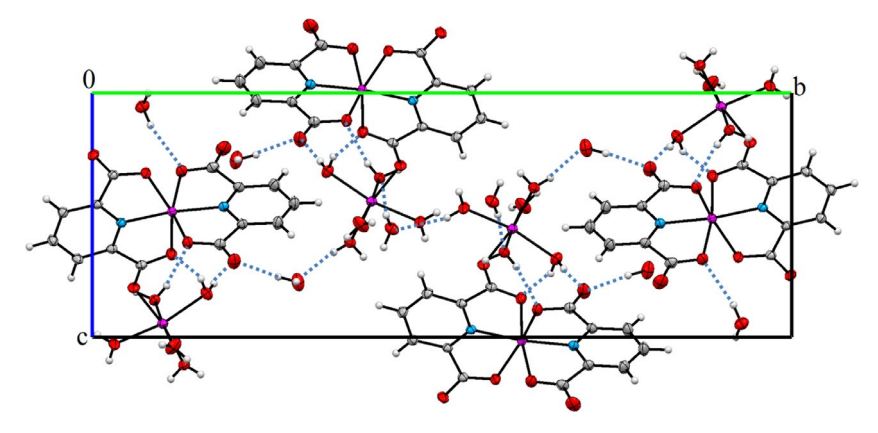


Fig. 5. A partial view of the crystal packing for complex 2. The dashed lines denote the intermolecular O -H ···O hydrogen bonds parallel to bc plane.

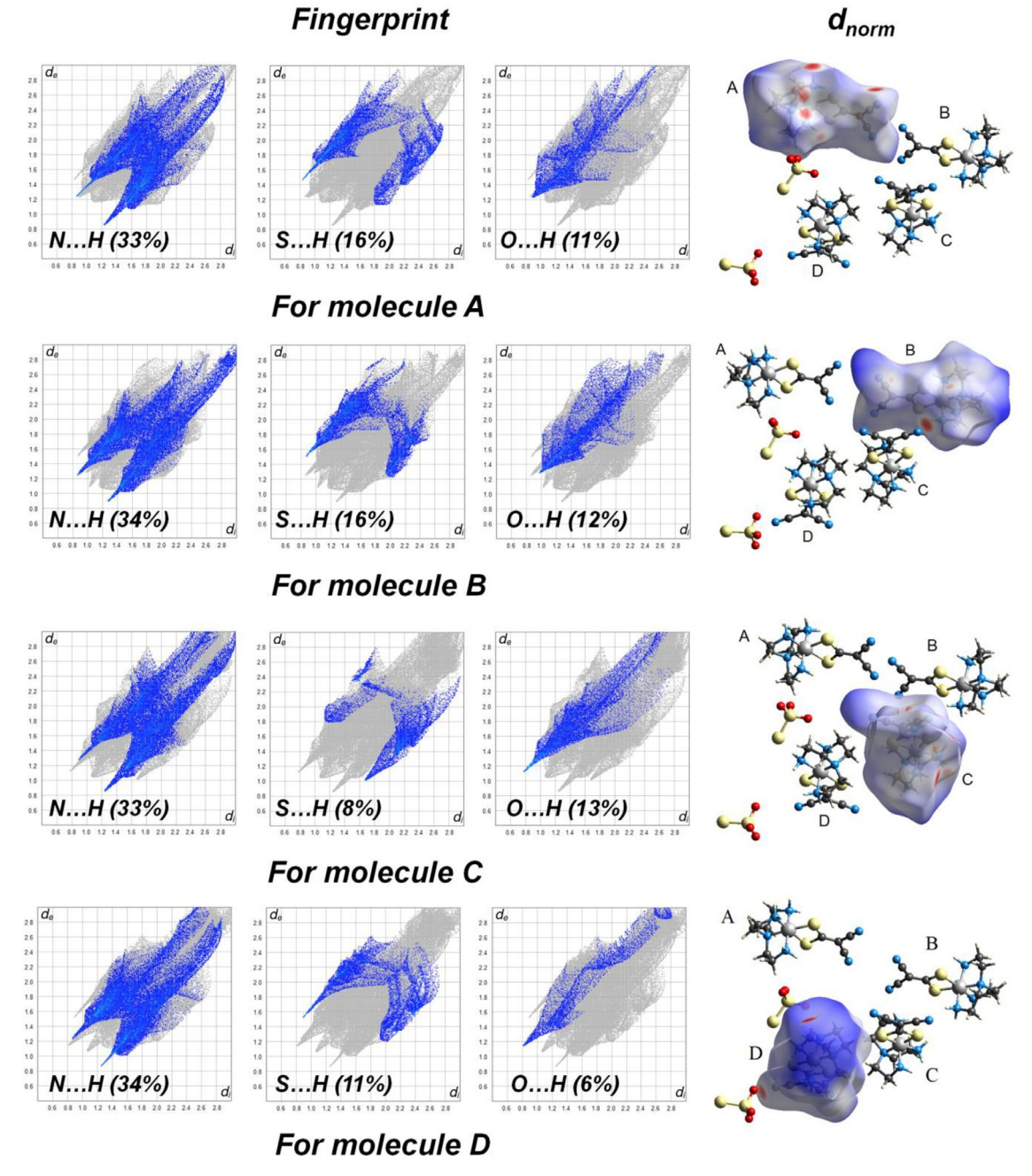


Fig. 6. Hirshfeld surfaces and fingerprints of 1 mapped with d

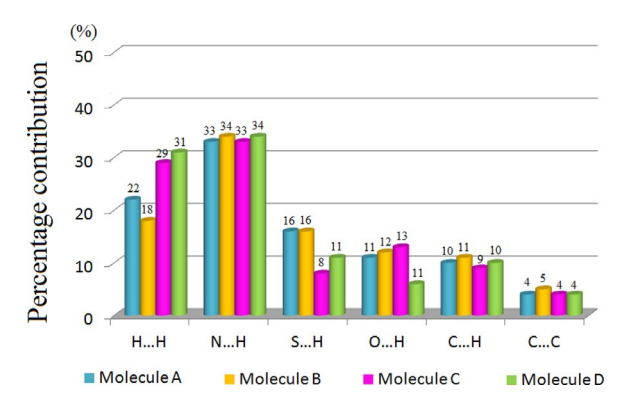


Fig. 7. Intermolecular interactions and their percentages for molecules A, B, C, and D in 1.

pated for a spin quartet  $(X_m T = 1.87 \text{ cm}^3 \text{mol}^- 1 \text{ K}, \text{ for } S = 3/2 \text{ with } g = 2.0)$ . However, it matches with the values observed for octahedral Co(II) compounds having a strong first-order contribution of the orbital magnetic moment, typical of the  $^4T_{1g}$  ground state [73–76]. The  $X_m T$  values for  $\mathbf{1}$  remain constant at about 20 K and considerably decrease at lower temperatures, reaching 1.45 cm $^3$ mol $^-$ 1 K at about 1.8 K. The decrease of  $X_m T$  at lower temperatures could be due to the intermolecular antiferromagnetic exchange interaction as well as depopulation of higher-energy spin-orbit coupling levels of the six coordinated Co(II) metal centers [77,78]. Furthermore, for  $\mathbf{1}$ , at low temperatures, there is no maximum molar susceptibility. In the solid-state, strong antiferromagnetic interactions can, therefore, be ruled out. Both in the presence and absence of applied static fields, there were no alternating current magnetic susceptibility signals.

The Curie and Weiss constant values were calculated using the relationship  $X_{\rm m}^{-1}$  = f( $^{7}$ ). The calculated Curie constant value for **1** is 2.38 cm³mol  $^{-}$ 1 K. The negative Weiss temperature is comparatively small ( $^{\theta}$  = -1.3 K). The result of non-zero Curie–Weiss temperature, being reported herein, probably replicates the decrease of  $X_{\rm m}^{T}$  with decreasing temperature that is attributable to the spin–orbit coupling instead of the frail antiferromagnetic interaction [73].

In order to investigate the ground state of **1**, we looked into how the magnetization, M, varied with the applied magnetic field at temperatures of 2, 4, 6, and 8 K. The outcomes are displayed in **Fig. S4** where the molar magnetization M (per  $\mathrm{Co^{II}}$  unit) is represented in  $\mu_B$  units. In the chosen range of applied fields, the complex does not attain saturation, and the magnetization at 7 T (2 K) is around  $2.7\mu_B$ . For one uncoupled  $\mathrm{Co(II)}$  ion in the S=3/2 ground state with g=2 and no zero-field splitting, the shape of the experimental plot for **1** does not obey the Brillouin function. This type of behavior may be a result of the  $\mathrm{Co^{II}}$  ions' magnetic anisotropy and/or the weak intermolecular antiferromagnetic interaction at low temperatures.

The S=3/2 state is divided into two Kramer's doublets ( $M_S=\pm 1/2$  and  $\pm 3/2$ ) due to spin-orbit coupling, with a distance of 2D between them, where D is the axial zero-field splitting parameter. Under the influence of the spin Hamiltonian (Eq. (1)), the magnetic properties may be viewed as a S=3/2 spin-state, appropriate for depicting magnetic anisotropy [79]:

$$\hat{H} = D S_2^p - \frac{1}{3}S(S+1) + g\beta HS$$
 (1)

Eqs. (2)–(4) display the magnetic susceptibility for a magnetically isolated Co(II) ion resulting from this Hamiltonian [79]:

$$X_m = \frac{X_{//} + 2X}{3} \tag{2}$$

$$\chi_{II} = \frac{N\beta^2 g_{II}^2}{4kT} \cdot \frac{1 + 9\exp{-\frac{2D}{kT}}}{1 + \exp{-\frac{2D}{kT}}}$$
(3)

$$\chi = \frac{N\beta^2 g^2}{4kT} \cdot \frac{4 + 3\frac{kT}{D} - 1 - \exp{-\frac{2D}{kT}}}{1 + \exp{-\frac{2D}{kT}}}$$
(4)

Taking into account the possibility of the presence of weak intermolecular magnetic interaction, the Eq. (2) must be redefined by involving a molecular field rectification term zJ'[79]. This yields the equation (Eq. (5)):

$$X_m^{corr} = \frac{X_m}{1 - \frac{2^{zJ}}{NB^2\sigma^2} \cdot X_m}$$
 (5)

Here, Z is the number of closest neighbours surrounding a certain magnetic species in the crystal system and J' is the interaction parameter between two closest neighbor magnetic species. To avoid over-parameterization, we ignored the rhombic zero-field splitting components and took into account  $g_{\parallel} = g_{\perp} = g$  (average Landé factor) during the fitting process. The values obtained from the best fit are: |D| = 25.5(1) cm<sup>-1</sup> (the sign of D cannot be inferred from the data on powder magnetic susceptibility), zJ' = -0.21(2) cm<sup>-1</sup> and g = 2.31(1) for **1**. The best fit was determined by using the criterion  $R = (\chi_{exp} T - \chi_{calc} T)^2 / (\chi_{exp} T)^2$  $(R = 4.42 \times 10^{-4})$ , which is based on diminishing the sum of squares of the deviation. In the entire temperature range, the computed curve for 1 (solid line in Fig. 11) closely fits the experimental data. The value of D falls in the range of similar magnetostructurally studied Co(II) compounds that have been reported [80-82]. Due to the relatively large distance between the paramagnetic Coll ions in the crystal structure (average Co...Co distances are 5.95 Å), value of ZJ' in **1** is very low, which indicates that there are very little intermolecular magnetic interactions. The computed D parameter, however, indicates that in 1, large magnetic anisotropy is dominating because of its substantially larger value as compared to zJ'.

In contrast to compound  ${\bf 1}$ , compound  ${\bf 2}$  is a dinuclear cobalt(II) complex. The magnetic characteristics of  ${\bf 2}$  are depicted

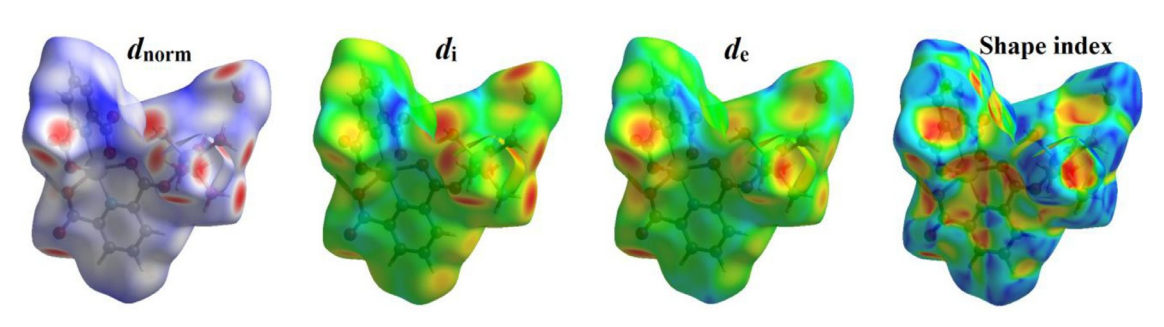


**Fig. 8.** Hirshfeld surfaces of 1, mapped with  $d_{\text{norm}}$ ,  $d_{\text{i}}$ ,  $d_{\text{e}}$ , and shape index.

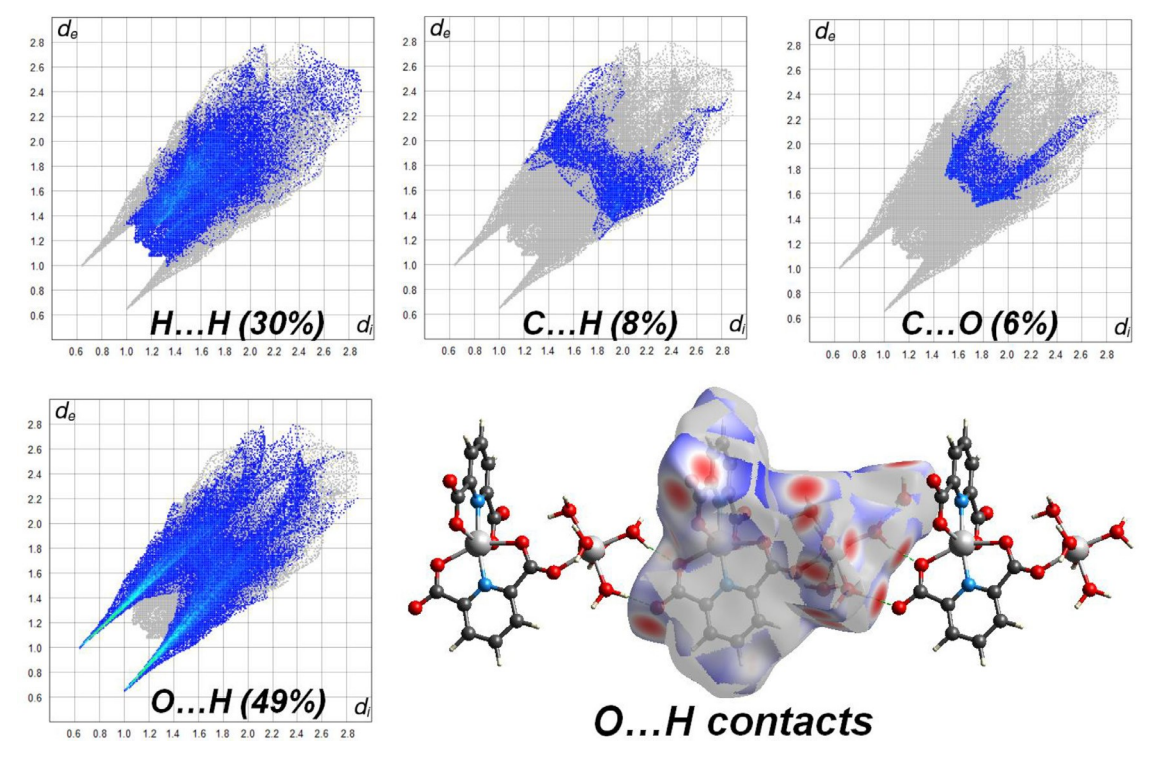
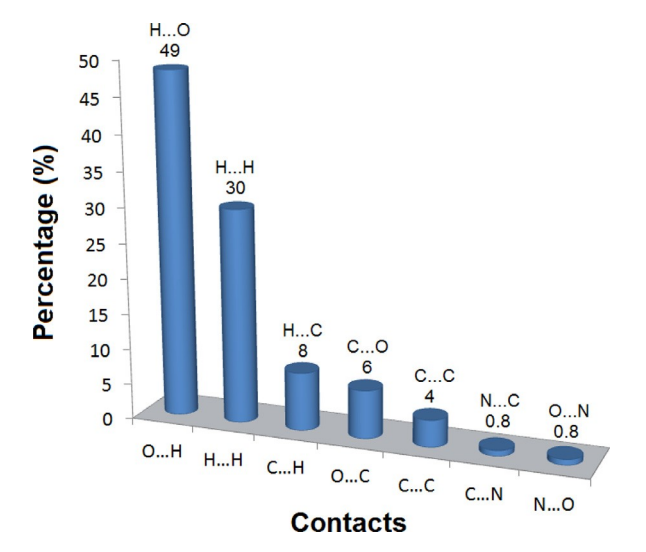
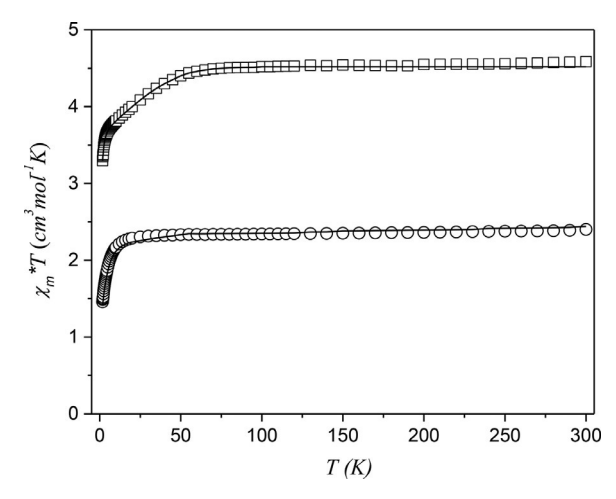


Fig. 9. Hirshfeld surface analyses of 2, mapped with d norm showing O −H ···O hydrogen-bonded contacts.



 $\textbf{Fig. 10.} \ \ \textbf{Intermolecular interactions and their percentage contributions for 2.}$ 

in Fig. 11 as a  $X_m^T$  against  $^T$  plot ( $X_m$  is the magnetic susceptibility per two  $^{\rm Co}$  ions). The measured  $X_m^T$  value at 300 K is 4.63 cm $^3$ mol $^-$ 1 K, which is higher than the spin only value of 3.75 cm $^3$ mol $^-$ 1 K for two uncoupled  $^S$  = 3/2 spins (g = 2.0). This is explained by the unquenched orbital angular momentum caused by the cobalt(II) ion's  $^4T_{1g}$  ground state [83]. Upon cooling, the  $X_m^T$  value decreases very slowly in the temperature range of 300–50 K but does so sharply in the temperature range of 50–1.8 K to attain the lowest value of 3.35 cm $^3$ mol $^-$ 1 K at 1.8 K. The decrease of magnetic moment with the lowering of temperature can be explained on the basis of three factors,  $^{ViZ}$ .: (i) orbital angular momentum contribution, (ii) a two-cobalt(II) intramolecular antiferromagnetic coupling, and (iii) an antiferromagnetic intermolecular coupling. Since the dinuclear cobalt(II) ions entities are far



**Fig. 11.** Temperature dependence of experimental c = mT (°) ( $X_m$  per Co  $^{\parallel}$  unit) for 1 and  $c_mT$  () ( $X_m$  per Co  $^{2}$  unit) for 2. The solid lines are the calculated curves obtained from Eqs. (2)–(5) for 1 and Eqs. (6), (7) for 2.

apart from one another, the intermolecular interactions may be neglected. A fit of  $\chi_{\rm m}^{-1}$ , at temperature values higher than 50 K, to the Curie–Weiss law yields a Curie constant ( $^{\rm C}$ ) value of 4.65 cm $^{\rm 3}$ Kmol $^{\rm -1}$  and a Weiss temperature ( $^{\rm H}$ ) value of -1.9 K. A weak antiferromagnetic interaction inside the Co(II)-Co(II) dinuclear unit is further indicated by the negative value of the Weiss temperature. As no maximum is observed in the  $\chi_{\rm m}$  vs.  $^{\rm T}$  plot until 1.8 K, the thermal dependence of  $\chi_{\rm m}$  is indicative of a weak antiferromagnetic interaction. Similar to 1, there are no signs for magnetic susceptibility for alternating current in case of 2.

Magnetization studies in the temperature range of 2–8 K confirmed the ground state nature of **2** (Fig. S5). With a magnetization value of  $\sim 3.6 \, \mu_{\rm B}$  at 7 T at 2 K, the compound does not reach saturation in the M vs. H measurements. Even at 7 T and 2 K, the magne-

tization is less than what is expected for a two uncoupled S=3/2 systems (with g=2) due to the absence of zero-field splitting. The experimental data do not precisely obey the Brillouin formula for **2**. The experimental data at intermediate magnetic field values are well below the theoretical curve, indicating a weak antiferromagnetic interaction.

As the orbital angular momentum contribution is absent in the ground state term, the spin-only method may be appropriate for this system when considering the distorted octahedral geometry of the high-spin cobalt(II) cations in **2** [77,78,84,85]. The decrease of  $X_m T$  in the temperature region of 300–1.8 K implies the presence of intramolecular antiferromagnetic interactions and in such a case, the Heisenberg–Van Vleck spin Hamiltonian (Eq. (6)) for an S = 3/2

dimer can be used as a simplification [77,78]:

$$\hat{H} = -2 \, J S_1 \cdot S_2 \tag{6}$$

Eq. (7) was used to fit the magnetic data [77-79] .

$$X_{m} = \frac{2N\beta^{2}g^{2}}{kT} \cdot \frac{14\exp{-\frac{12J}{kT}} + 5\exp{-\frac{6J}{kT}} + \exp{-\frac{2J}{kT}}}{7\exp{-\frac{12J}{kT}} + 5\exp{-\frac{6J}{kT}} + 3\exp{-\frac{3J}{kT}} + 1}$$
(7)

Here, J is the intradimer interaction parameter (exchange coupling constant) between  $Co^{II}$  ions. The best fit of the data utilizing the above-mentioned equation for **2** results in J = -1.21(2) cm<sup>-1</sup> and g = 2.35(1) ( $R = 8.37 \times 10^{-4}$ ), as demonstrated by the solid curve in Fig. 11. In the entire temperature range, the experimental results are reproducible. The  $Co_2$  unit exhibits weak an-

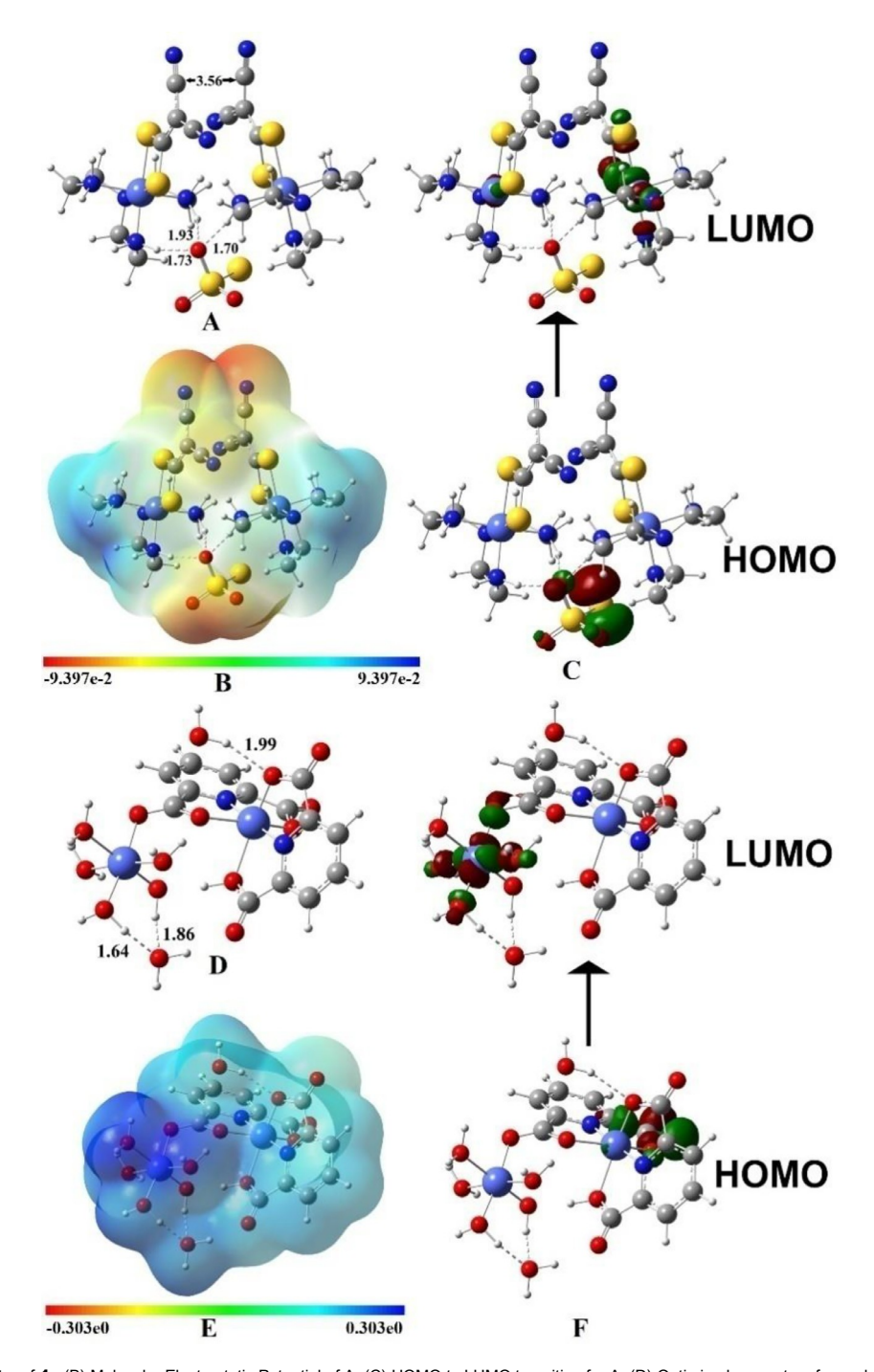


Fig. 12. (A) Optimized geometry of 1, (B) Molecular Electrostatic Potential of A, (C) HOMO to LUMO transition for A, (D) Optimized geometry of complex 2, (E) Molecular Electrostatic Potential of B, and (F) HOMO to LUMO transition for D.

tiferromagnetic interaction, as indicated by the negative J value. Other structurally significant dinuclear cobalt(II) complexes have also exhibited antiferromagnetic coupling interactions, and the observed J values for such complexes have magnitudes [101] close to that reported for 2. As mentioned previously, the kind of bridging mode, the Cu---Cu separations, the coordination arrangement of Cu(II) centers, and the bond angles of bridging ions, all affect the magnitude and sign of J in carboxylato-based Cu(II) complexes [86,87]. Because of the complexities arising from the orbital angular momentum contributions, which are highly reliant on the coordination geometry as well as the ligand field surrounding the metal center, magneto-structural correlation for the cobalt(II) complexes is still unclear [88,89]. However, taking into account that the Co1-O-C-O-Co2 backbone in 2 deviates from planarity, the overlap among the magnetic orbitals of both cobalt (II) ions via the syn-anti carboxylate linkage is appreciably frail and results in weak antiferromagnetic interactions.

### 3.6. DFT study

Fig. 12A represents the optimized geometry of **1**. The two  $C_{10}H_{18}CoN_6S_2$  units are held together by  $S_2O_3^{2-}$  group via H-bond formation with a distance of 1.70 to 1.93 Å between them and by  $\pi \cdots \pi$  stacking with a distance of 3.56 Å between the units with a Co-Co distance of 5.95 Å. Fig. 12B represents molecular electrostatic potential (MEP) of **1**. From Fig. 12B, it is clear that stacking

occurs via two cyanide groups indicated by red regions. The electronic transition from HOMO to LUMO is shown in Fig. 12C with a band gap of 2.37 eV. The charge is transferred from S<sub>2</sub>O<sub>3</sub><sup>2-</sup> to metal, suggesting strong chelation. Fig. 12D represents optimized geometry of 2. Here, water molecules are coordinated to cobalt (II) to satisfy the valency of the latter and also to stabilize the crystal with a Co-Co distance of 4.78 Å. MEP plot for 2, shown in Fig. 12E, suggests that H-bonding interactions are the only stabilizing factor for the crystal. Electronic transition with a band gap of 1.90 eV has been shown in Fig. 12F. The charge-transfer occurs from oxygen to metal, which revealed the donor-acceptor HOMO-LUMO modeling for prediction of crystal formation. Low magnetic moment values of 0.55 and 0.52 BM per atom for 1 and 2, respectively, were found. Magnetic susceptibility values of -63.82 and -19.36 au were observed for 1 and 2, respectively, which indicates their aniferromegnetic behavior; these findings are in concordance with the experimental results.

### 3.7. Electrochemical analysis

Cyclic voltammetry was performed on a CH-Instruments Electrochemical Analyzer 600C potentiostat, equipped with three electrodes: glassy carbon as working, platinum as counter, and silver (Ag/AgCl) as reference. Solutions of both the compounds were prepared in dry DMSO to a concentration of 1 mM, with 0.1 M tetrabutylammonium hexafluorophosphate as the electrolyte.

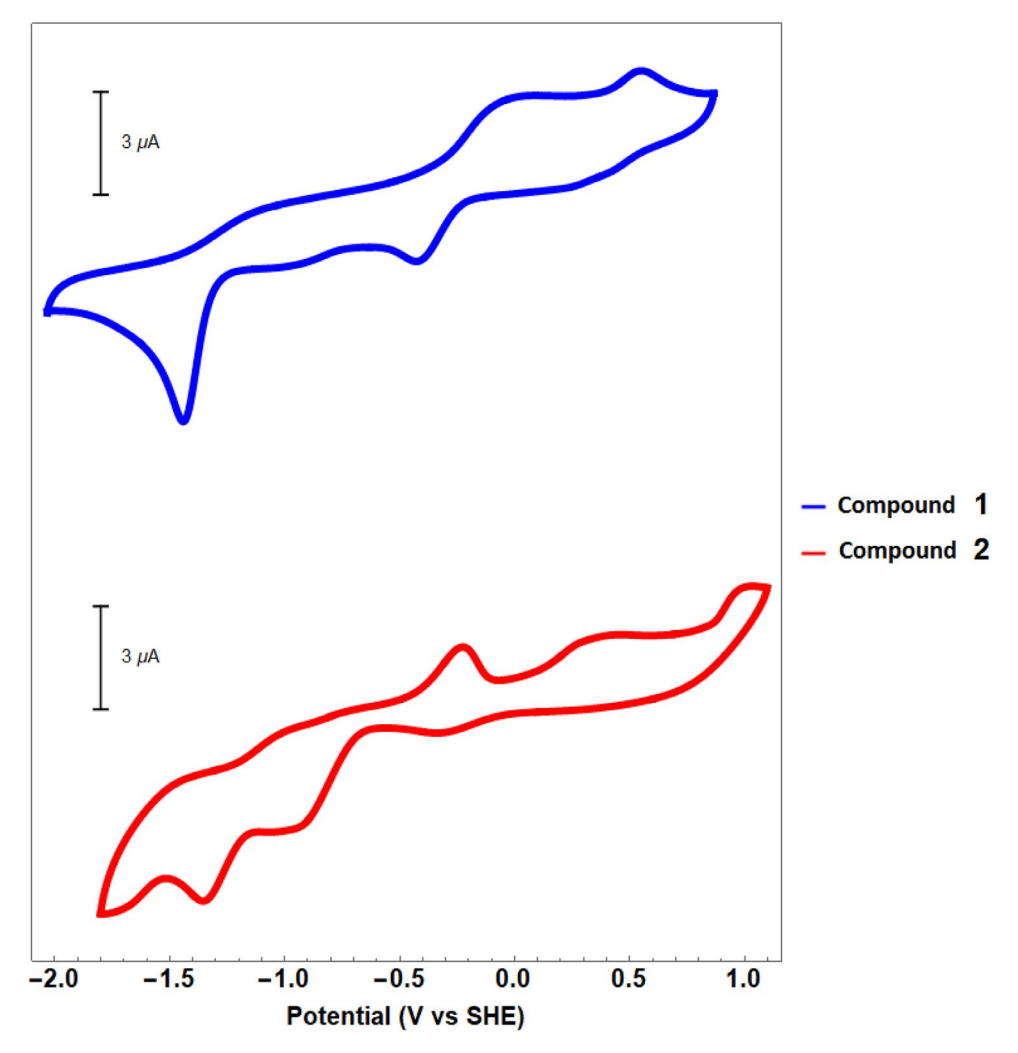


Fig. 13. Cyclic voltammograms recorded in dry DMSO for both the compounds corrected by the introduction of an internal standard.

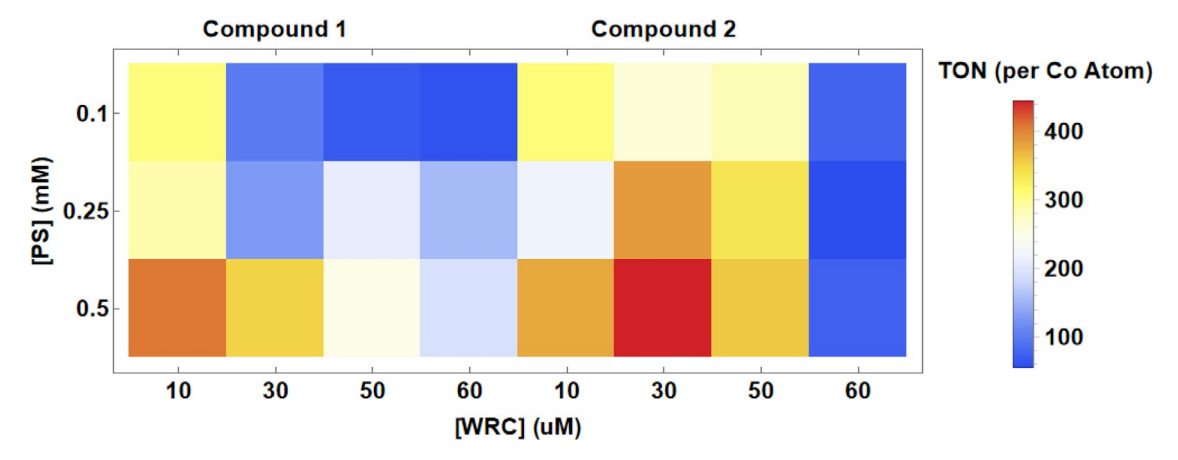


Fig. 14. TON per Co atom for the production of hydrogen in photocatalytic water reduction presented for various PS and WRC concentration combinations.

Cyclic voltammetric scans were recorded in a potential range of -2.0 to +0.9 V, and were adjusted to the standard hydrogen electrode (SHE) by the introduction of an internal standard, ferrocene. Compound 1 revealed a non-reversible reduction peak at -1.42 V, while 2 revealed two non-reversible reduction peaks at -1.35 and -1.78 V (Fig. 13). Moving to acetonitrile as an electrolyte solvent documented that 1 does not undergo solvent exchange under these conditions and the CVs show only minor changes. Compound 2, on the other hand, exhibits a current response that was diminished by a factor of 2 and some of peaks disappeared, indicating the susceptibility of this compound to solvent exchange.

### 3.8. Photocatalytic hydrogen evolution

Using the high throughput photoreactor, the two compounds were tested for their water reduction capabilities. Concentration was gradated in two dimensions, by variation of PS and WRC concentrations by either column or row, respectively (Fig. 14). The results demonstrate that the catalysts are highly efficient in terms of turn-over-numbers (TON) per Co when they are at lower concentration with higher concentration of PS. Comparison of rates of light-driven hydrogen evolution of the two compounds against standard cobalt containing systems can be found in the Supporting Information (Figs. S10 and S11).

### 4. Conclusions

In this work, we have successfully synthesized two cobalt (II)based coordination complexes 1 and 2, which exhibit supramolecular assemblies. In 1, the X-ray structure analysis discloses the coordination of Co1 ion to four enamine nitrogen atoms of ligand tetraen and two sulfur atoms of i-mnt 2- ligand, creating a distorted octahedral geometry. The Co2, Co3, and Co4 atoms have similar geometries. The thiosulphate ions act as connector between two cobalt(II) centers. The two thiosulphate ions and Co(II) ions are connected via intermolecular hydrogen bonding. In compound 2, the dicarboxylate ligand acts as a teteradentate ligand and the two Co (II) centers are joined by carboxylate bridging ligand. HS analyses decoded the different types of noncovalent interactions, which play important roles for stabilizing the crystal structures of both the coordination compounds. For 1, the most significant contributions to the Hirshfeld surface are N···H, H···H, S···H, and O···H interactions. In case of 2, the outcome of the investigation show that the O···H (49%) contacts are the most prominent ones, whereas H···H (30%) and C···H (8%) contacts are less noteworthy. Magnetic susceptibility measurement results for 1 suggests that the effect of zero-field splitting of Coll ion is mainly responsible for

the decrease of magnetic moment at low temperatures. The magnetic studies of **2** point out the presence of weak intermolecular exchange interactions. The HOMO-LUMO donor-acceptor modeling revealed from DFT study also supports for prediction of crystal formation. Cyclic voltammetry confirmed non-reversible reduction peaks beyond -1 V (vs. SHE) for both the complexes. Furthermore, photocatalytic hydrogen evolution testing resulted in the conclusion that both the complexes perform highly efficiently at lower concentrations resulting in TON per Co Atom of up to 325.

### **Declaration of Competing Interest**

The authors declare that they have no known competing financial interests or personal relationships that could have appeared to influence the work reported in this paper.

### CRediTauthorshipcontributionstatement

Suman Adhikari: Conceptualization, Investigation, Writing – original draft, Supervision. SevgiKansız:Investigation, Writing – original draft. NecmiDege:Investigation, Writing – original draft. NabajyotBaildya:Investigation, Writing – original draft. Ghodrat Mahmoudi: Conceptualization, Investigation. Nurul Alam Choudhury: Investigation. RaymondJ. Butcher: Investigation. Werner Kaminsky:Investigation. SavannahTalledo:Investigation. Eric M. Lopato:Investigation. StefanBernhard:Conceptualization, Investigation, Writing – original draft. JuliaKłak:Investigation, Writing – original draft.

### **Dataavailability**

No data was used for the research described in the article.

# Acknowledgements

The author is grateful to Prof. Kumaresh Ghosh, Department of Chemistry, University of Kalyani, Nadia, India, for spectral analysis.

## Supplementarymaterials

Supplementary material associated with this article can be found, in the online version, at doi:10.1016/j.molstruc.2023.135481.

### References

[1] S.J. Bao, Z.M. Xu, Y. Ju, Y.L. Song, H. Wang, Z. Niu, X. Li, P. Braunstein, J.P. Lang, The covalent and coordination co-driven assembly of supramolecular octahedral cages with controllable degree of distortion, J. Am. Chem. Soc. 142 (31) (2020) 13356–13361.

- [2] H.A. Nkabyo, I. Barnard, K.R. Koch, R.C. Luckay, Recent advances in the coordination and supramolecular chemistry of monopodal and bipodal acylthiourea-based ligands, Coord. Chem. Rev. 427 (2021) 213588.
- [3] G.E. Decker, G.R. Lorzing, M.M. Deegan, E.D. Bloch, MOF-mimetic molecules: carboxylate-based supramolecular complexes as molecular metal-organic framework analogues, J. Mater. Chem. A 8 (8) (2020) 4217–4229.
- [4] J. Gu, M. Wen, X. Liang, Z. Shi, M.V. Kirillova, A.M. Kirillov, Multifunctional aromatic carboxylic acids as versatile building blocks for hydrothermal design of coordination polymers, Crystals 8 (2) (2018) 83.
- [5] G. Moreno-Alcántar, L. Turcio-García, J.M. Guevara-Vela, E. Romero-Montalvo, T. Rocha-Rinza, Á.M. Pendás, M. Flores-Álamo, H. Torrens, Directing the crystal packing in triphenylphosphine gold (I) thiolates by ligand fluorination, Inorg. Chem. 59 (13) (2020) 8667–8677.
- [6] M.R. Carlson, D.L. Gray, C.P. Richers, W. Wang, P.H. Zhao, T.B. Rauchfuss, V. Pelmenschikov, C.C. Pham, L.B. Gee, H. Wang, Sterically stabilized terminal hydride of a diiron dithiolate, Inorg. Chem. 57 (4) (2018) 1988–2001.
- [7] G. Li, M.F. Mark, H. LV, D.W. McCamant, R. Eisenberg, Rhodamine-platinum diimine dithiolate complex dyads as efficient and robust photosensitizers for light-driven aqueous proton reduction to hydrogen, J. Am. Chem. Soc. 140 (7) (2018) 2575–2586.
- [8] D. Coucouvanis, The chemistry of the dithioacid and 1, 1-dithiolate complexes, 1968–1977, Prog. Inorg. Chem. (1979) 301–469.
- [9] G. Hogarth, K. Karlin, In Progress in Inorganic Chemistry, Wiley Hoboken, NJ, 2005
- [10] S. Naeem, L. Delaude, A.J. White, J.D. Wilton-Ely, The use of imidazolium-2-dithiocarboxylates in the formation of gold (I) complexes and gold nanoparticles, Inorg. Chem. 49 (4) (2010) 1784–1793.
- [11] M.K. Singh, S. Sutradhar, B. Paul, S. Adhikari, F. Laskar, R.J. Butcher, S. Acharya, A. Das, A new cadmium (II) complex with bridging dithiolate ligand: synthesis, crystal structure and antifungal activity study, J. Mol. Struct. 1139 (2017) 335–399.
- [12] M.K. Singh, S. Sutradhar, B. Paul, S. Adhikari, F. Laskar, S. Acharya, D. Chakraborty, S. Biswas, A. Das, S. Roy, Mixed-ligand complexes of zinc (II) with 1, 1-dicyanoethylene-2, 2-dithiolate and N-donor ligands: a combined experimental and theoretical study, J. Mol. Struct. 1164 (2018) 334–343.
- [13] S. Adhikari, T. Bhattacharjee, R.J. Butcher, M. Porchia, M. De Franco, C. Marzano, V. Gandin, F. Tisato, Synthesis and characterization of mixed-ligand Zn (II) and Cu (II) complexes including polyamines and dicyano-dithiolate (2-): in vitro cytotoxic activity of Cu (II) compounds, Inorg. Chim. Acta 498 (2019) 119098.
- [14] S. Adhikari, T. Bhattacharjee, P. Nath, A. Das, J.P. Jasinski, R.J. Butcher, D. Maiti, Bimetallic and trimetallic Cd (II) and Hg (II) mixed-ligand complexes with 1, 1-dicyanoethylene-2, 2-dithiolate and polyamines: synthesis, crystal structure, Hirshfeld surface analysis, and antimicrobial study, Inorg. Chim. Acta (512) (2020).
- [15] S. Adhikari, T. Bhattacharjee, A. Das, S. Roy, C.G. Daniliuc, J.K. Zar eba, A. Bauza, A. Frontera, On the supramolecular properties of neutral, anionic and cationic cadmium complexes harvested from dithiolate–polyamine binary ligand systems, CrystEngComm 22 (46) (2020) 8023–8035.
- [16] T. Bhattacharjee, S. Adhikari, R.J. Butcher, Supramolecular properties directed by weak interactions in a copper (II) complex based on 8-hydroxy quinoline-pyridine binary ligand systems: crystal structure and hirshfeld surface analyses, J. Chem. Crystallogr. (2021) 1–12.
- [17] T. Bhattacharjee, S. Adhikari, A. Datta, C.G. Daniliuc, M. Montazerozohori, R. Naghiha, P. Hayati, Cadmium (II) coordination polymer based on flexible dithiolate-polyamine binary ligands system: crystal structure, Hirshfeld surface analysis, antimicrobial, and DNA cleavage potential, Polyhedron 211 (2022) 115544.
- [18] T. Bhattacharjee, S. Adhikari, A.H. Sheikh, G. Mahmoudi, S. Mlowe, M.P. Ak-erman, N.A. Choudhury, S. Chakraborty, R.J. Butcher, A.R. Kennedy, Syntheses, crystal structures, theoretical studies, and anticancer properties of an unsymmetrical schiff base ligand N-2-(6-methylpyridyl)-2-hydroxy-1-naphthaldimine and its Ni (II) complex, J. Mol. Struct. 1269 (2022) 133717.
- [19] S.C. Zacharias, G. Ramon, S.A. Bourne, Supramolecular metallogels constructed from carboxylate gelators, Soft Matter 14 (22) (2018) 4505–4519.
- [20] Q. Wang, S.L. Dong, D.D. Tao, Z. Li, Y.B. Jiang, Ag (I)-thiolate coordination polymers: synthesis, structures and applications as emerging sensory ensembles, Coord. Chem. Rev. 432 (2021) 213717.
- [21] S. Vela, M. Deumal, J. Ribas-Arino, J.J. Novoa, Tracing the sources of the different magnetic behavior in the two phases of the bistable (BDTA) 2 [Co (mnt) 2] compound, Inorg. Chem. 51 (16) (2012) 8646–8648.
- [22] A. K. Mondal, A. Mondal, B. Dey, S. Konar, Influence of the coordination environment on easy-plane magnetic anisotropy of pentagonal bipyramidal cobalt (II) complexes, Inorg. Chem. 57 (16) (2018) 9999–10 0 08.
- [23] J.W. Shin, A.R. Jeong, S.Y. Lee, C. Kim, S. Hayami, K.S. Min, Trinuclear nickel and cobalt complexes containing unsymmetrical tripodal tetradentate ligands: syntheses, structural, magnetic, and catalytic properties, Dalton Trans. 45 (36) (2016) 14089–14100.
- [24] D. Maniaki, E. Pilichos, S.P. Perlepes, Coordination clusters of 3d-metals that behave as single-molecule magnets (SMMs): synthetic routes and strategies, Front. Chem. 6 (2018) 461.
- [25] J.H. Wang, Z.Y. Li, M. Yamashita, X.H. Bu, Recent progress on cyano-bridged transition-metal-based single-molecule magnets and single-chain magnets, Coord. Chem. Rev. 428 (2021) 213617.
- [26] S. Ghosh, S. Kamilya, M. Das, S. Mehta, M.E. Boulon, I. Nemec, M. Rouzieres, R. Herchel, A. Mondal, Effect of coordination geometry on magnetic properties

- in a series of cobalt (II) complexes and structural transformation in mother liquor, Inorg. Chem. 59 (10) (2020) 7067–7081.
- [27] J. Wang, J.N. Li, S.L. Zhang, X.H. Zhao, D. Shao, X.Y. Wang, Syntheses and magnetic properties of a pyrimidyl-substituted nitronyl nitroxide radical and its cobalt (II) complexes. Chem. Commun. 52 (28) (2016) 5033–5036.
- [28] H.B. Gray, Powering the planet with solar fuel, Nat. Chem. 1 (1) (2009) 7-7
- [29] J. Corredor Ortega, New strategies in the generation of photocatalytic hydrogen, (2021).
- [30] Y. Shi, A.F. Yang, C.S. Cao, B. Zhao, Applications of MOFs: recent advances in photocatalytic hydrogen production from water, Coord. Chem. Rev. 390 (2019) 50–75.
- [31] W.R. McNamara, Z. Han, P.J. Alperin, W.W. Brennessel, P.L. Holland, R. Eisenberg, A cobalt-dithiolene complex for the photocatalytic and electrocatalytic reduction of protons, J. Am. Chem. Soc. 133 (39) (2011) 15368–15371.
- [32] M. Natali, A. Luisa, E. lengo, F. Scandola, Efficient photocatalytic hydrogen generation from water by a cationic cobalt (II) porphyrin, Chem. Commun. 50 (15) (2014) 1842–1844.
- [33] P. Zhang, M. Wang, F. Gloaguen, L. Chen, F. Quentel, L. Sun, Electrocatalytic hydrogen evolution from neutral water by molecular cobalt tripyridine–diamine complexes, Chem. Commun. 49 (82) (2013) 9455–9457.
- [34] R.W. Hogue, O. Schott, G.S. Hanan, S. Brooker, A smorgasbord of 17 cobalt complexes active for photocatalytic hydrogen evolution, Chem. A Eur. J. 24 (39) (2018) 9820–9832.
- [35] K.T. Mahmudov, M.N. Kopylovich, M.F.C.G. da Silva, A.J. Pombeiro, Non-covalent interactions in the synthesis of coordination compounds: recent advances, Coord. Chem. Rev. 345 (2017) 54–72.
- [36] J. Lehn, Concept and perspectives, Supramol. Chem. (1995)
- [37] S. Adhikari, D. Kar, R. Fröhlich, K. Ghosh, Pyridine-based macrocyclic and open receptors for urea, ChemistrySelect 4 (44) (2019) 12825–12831.
- [38] I.W. Park, J. Yoo, S. Adhikari, J.S. Park, J.L. Sessler, C.H. Lee, Calix [4]pyrrole-based heteroditopic ion-pair receptor that displays anion-modulated, cation-binding behavior, Chem. A Eur. J. 18 (47) (2012) 15073–15078
- [39] K. Ghosh, S. Adhikari, R. Fröhlich, A pyridine-based macrocyclic host for urea and acetone, Tetrahedron Lett. 49 (34) (2008) 5063–5066.
- [40] K. Ghosh, S. Adhikari, R. Fröhlich, I.D. Petsalakis, G. Theodorakopoulos, Experimental and theoretical anion binding studies on coumarin linked thiourea and urea molecules, J. Mol. Struct. 1004 (1–3) (2011) 193–203.
- [41] I.W. Park, J. Yoo, B. Kim, S. Adhikari, S.K. Kim, Y. Yeon, C.J. Haynes, J.L. Sutton, C.C. Tong, V.M. Lynch, Oligoether-strapped calix [4]pyrrole: an ion-pair receptor displaying cation-dependent chloride anion transport, Chem. A Eur. J. 18 (9) (2012) 2514–2523.
- [42] K. Ghosh, S. Adhikari, A.P. Chattopadhyay, P.R. Chowdhury, Quinoline based receptor in fluorometric discrimination of carboxylic acids, Beilstein J. Org. Chem. 4 (1) (2008) 52.
- [43] K. Jensen, L. Henriksen, Studies of thioacids and their derivatives, Acta Chem. Scand. 22 (1968) 1107–1128.
- [44] Y. Qi, Y. Wang, H. Fan, M. Cao, L. Mao, C. Hu, E. Wang, N. Hu, H. Jia, Structure characterization and physical properties of a complex with supramolecular architectures Co2 (2, 6-DPC) 2Co (H2O) 5 · 2H2O (DPC 2, 6-pyridinedicarboxylate), J. Mol. Struct. 694 (1–3) (2004) 73–78.
- [45] BrukerAPEX3 and SAINT, Bruker AXS Inc., Madison, Wisconsin, USA, 2017
- [46] G. Sheldrick, Using phases to determine the space group, Acta Crystallogr. A 74 (2018) a353.
- [47] G.M. Sheldrick, Crystal structure refinement with SHELXL, Acta Crystallogr Sect. C Struct. Chem. 71 (1) (2015) 3–8.
- [48] L. Krause, R. Herbst-Irmer, G.M. Sheldrick, D. Stalke, Comparison of silver and molybdenum microfocus X-ray sources for single-crystal structure determination, J. Appl. Crystallogr. 48 (1) (2015) 3–10.
- [49] M.A. Spackman, D. Jayatilaka, Hirshfeld surface analysis, CrystEngComm 11 (1) (2009) 19–32 .
- [50] M. Turner, J. McKinnon, S. Wolff, D. Grimwood, P. Spackman, D. Jayatilaka, M. Spackman, CrystalExplorer (Version 17.5), University of Western Australia: Crawley, Australia, 2017.
- [51] M. Frisch, G.W. Trucks, H.B. Schlegel, G.E. Scuseria, M.A. Robb, J.R. Cheeseman, G. Scalmani, V. Barone, B. Mennucci, G. Petersson, Gaussian 09, revision D. 01, Gaussian, Inc., Wallingford CT, 2009.
- [52] X. Qian, Y.Z. Zhu, J. Song, X.P. Gao, J.Y. Zheng, New donor-  $\pi$ -acceptor type triazatruxene derivatives for highly efficient dye-sensitized solar cells, Org. Lett. 15 (23) (2013) 6034–6037 .
- [53] G. Bain, J. Berry, J. Chem. Educ. 85 (4) (2008) 532-536
- [54] E.M. Lopato, E.A. Eikey, Z.C. Simon, S. Back, K. Tran, J. Lewis, J.F. Kowalewski, S. Yazdi, J.R. Kitchin, Z.W. Ulissi, Parallelized screening of characterized and DFT-modeled bimetallic colloidal cocatalysts for photocatalytic hydrogen evolution, ACS Catal. 10 (7) (2020) 4244–4252.
- [55] W. Song, E.M. Lopato, S. Bernhard, P.A. Salvador, G.S. Rohrer, High-throughput measurement of the influence of pH on hydrogen production from BaTiO 3/TiOs core/shell photocatalysts, Appl. Catal. B 269 (2020) 118750.
- [56] D. Avcı, S. Altürk, F. Sönmez, Ö. Tamer, A. Ba s ğilu, Y. Atalay, B.Z. Kurt, N. Dege, Novel Cu (II), Co (II) and Zn (II) metal complexes with mixed-ligand: synthesis, crystal structure, α-glucosidase inhibition, DFT calculations, and molecular docking, J. Mol. Struct. 1197 (2019) 645–655.
- [57] S. Altürk, D. Avcı, B.Z. Kurt, Ö. Tamer, A. Ba s ğılu, F. Sönmez, Y. Atalay, N. Dege, Two new Co (II) complexes of picolinate: synthesis, crystal structure, spectral characterization, α-glucosidase inhibition and TD/DFT study, J. Inorg. Organomet. Polym. Mater. 29 (4) (2019) 1265–1279.

- [58] A. J. Fischmann, A. C. Warden, J. Black, L. Spiccia, Synthesis, characterization, and structures of copper (II) – thiosulfate complexes incorporating tripodal tetraamine ligands, Inorg. Chem. 43 (21) (2004) 6568–6578.
- [59] E.Z. Dalton, W.R. Blomberg, E.M. Villa, Syntheses and structures of the first lanthanide–thiosulfate complexes and the subsequent formation of mixed thiosulfate–sulfite compounds, Cryst. Growth Des. 21 (5) (2021) 3071–3081.
- [60] A. Kufelnicki, S.V. Tomyn, V. Vitske, J. Jaciubek-Rosi ńska, M. Haukka, I.O. Fritsky, Synthesis, solid state and solution studies of cobalt (II) complexes with 2-hydroxyiminopropanoic acid, Polyhedron 56 (2013) 144–151.
- [61] K. Chkirate, K. Karrouchi, N. Dege, N.K. Sebbar, A. Ejjoummany, S. Radi, N. Adarsh, A. Talbaoui, M. Ferbinteanu, E.M. Essassi, Co (ii) and Zn (ii) pyrazolyl-benzimidazole complexes with remarkable antibacterial activity, New J. Chem. 44 (6) (2020) 2210–2221.
- [62] D.M. Al-thamili, A.I. Álmansour, N. Arumugam, S. Kansız, N. Dege, S.M. Soliman, M. Azam, R.S. Kumar, Highly functionalized N-1-(2-pyridinylmethyl)-3, 5-bis [(E)-arylmethylidene] tetrahydro-4 (1H)-pyridinones: synthesis, characterization, crystal structure and DFT studies, J. Mol. Struct. 1222 (2020) 128940
- [63] K. Karrouchi, S. Fettach, Ö. Tamer, D. Avci, A. Ba s oğlu, Y. Atalay, Z. Ayaz, S. Radi, H.A. Ghabbour, Y.N. Mabkhot, Synthesis, crystal structure, spectroscopic characterization, a-glucosidase inhibition and computational studies of (E)-5-methyl-N -(pyridin-2-ylmethylene)-1H-pyrazole-3-carbohydrazide, J. Mol. Struct. 1248 (2022) 131506.
- [64] A. J.M. Al-Karawi, AA.B. OmarAli, N. Dege, S. Kansız, Formation of a new Cull-triazole ester complex from 1, 2-cyclohexanedione-bis (p-bromobenzohydrazone) compound as a consequence of copper (II)-catalyzed click reaction, Chem. Pap. 75 (8) (2021) 3901–3914.
- [65] A. J.M. Al-Karawi, AA. B. OmarAli, S. Mangelsen, N. Dege, S. Kansız, P. Breuninger, C. Baydere, O.B. OmarAli, An unprecedented formation of new copper (II) complexes as bioactive materials based on copper-catalyzed click reaction, Polyhedron 198 (2021) 115084.
- [66] M. Azam, P.K. Sahoo, R.K. Mohapatra, M. Kumar, A. Ansari, I.S. Moon, A. Chutia, S.I. Al-Resayes, S.K. Biswal, Structural investigations, Hirsfeld surface analyses, and molecular docking studies of a phenoxo-bridged binuclear Zinc (II) complex, J. Mol. Struct. 1251 (2022) 132039.
- [67] M. Morales-Toyo, S. Kansız, N. Dege, C. Glidewell, A. Fuenmayor-Zafra, N. Cubillán, Polymorphs of 2-[2-[(2, 6-dichlorophenyl) amino] phenyl] acetic acid (Diclofenac): differences from crystallography, Hirshfeld surface, QTAIM and NCI-Plots, Chem. Phys. 544 (2021) 111119.
- [68] N.K. Ya ğcı, S. Kansız, E. Özcandan, Synthesis, crystal structure, DFT studies, Hirshfeld surface analysis and drug delivery performance of bis (2-chloro-4, 6-diaminopyrimidine) copper (II)-dichloride, J. Mol. Struct. 1246 (2021) 131142.
- [69] L.J. Daumann, P. Comba, J.A. Larrabee, G. Schenk, R. Stranger, G. Cavigliasso, L.R. Gahan, Synthesis, magnetic properties, and phosphoesterase activity of dinuclear cobalt (II) complexes, Inorg. Chem. 52 (4) (2013) 2029–2043.
- [70] H. Sakiyama, Amendment to "Magnetic susceptibility equation for dinuclear high-spin cobalt (II) complexes considering the exchange interaction between two axially distorted octahedral cobalt (II) ions"[Inorg. Chim. Acta 359 (2006) 2097–2100], Inorg. Chim. Acta 2 (360) (2007) 715–716.
- [71] F. Lloret, M. Julve, J. Cano, R. Ruiz-García, E. Pardo, Magnetic properties of six-coordinated high-spin cobalt (II) complexes: theoretical background and its application, Inorg. Chim. Acta 361 (12–13) (2008) 3432–3445.
- [72] S.Y. Lin, G.F. Xu, L. Zhao, J. Tang, G.X. Liu, Structure and Magnetic Properties of A μ-Phenoxido-bridged Dinuclear Cobalt (II) Complex, Wiley Online Library, 2011.

- [73] Y.H. Zhou, Z.Y. Wang, Four coordination polymers based on flexible carboxylic acid and bis (pyridyl) mixed ligands: synthesis, structures, fluorescent and magnetic properties, Transit. Met. Chem. 40 (1) (2015) 89–98.
- [74] C.Y. Sun, X.J. Zheng, S. Gao, L.C. Li, L.P. Jin, Multiple Regulated assembly, Crystal Structures and Magnetic Properties of Porous Coordination Polymers With Flexible Ligands, Wiley Online Library, 2005.
- [75] F.N. Figgis, J. Levis, Prog. Inorg. Chem. 6 (1964) 37 .
- [76] F.E. Mabbs, D.J. Machin, Magnetism and Transition Metal Complexes, Chapman and Hall, London, 1973, p. 7.
- [77] O. Kahn, in: Molecular Magnetism, VCH, Publishers Inc., New York, 1993, pp. 167–174.
- [78] O. Kahn, J. Larionova, J. Yakhmi, Molecular magnetic sponges, Chem. A Eur. J. 5 (12) (1999) 3443–3449.
- [79] O. Kahn, Magnetism of the heteropolymetallic systems, Theor. Approaches (1987) 89–167
- [80] R. Rabelo, A.K. Valdo, C. Robertson, J.A. Thomas, H.O. Stumpf, F.T. Martins, E.F. Pedroso, M. Julve, F. Lloret, D. Cangussu, Synthesis, crystal structure and magnetic properties of [Co (bpcam) 2] ClO 4 dmso · H<sub>2</sub>O,[Co (bpcam) 2]<sub>2</sub>[Co (NCS)<sub>k</sub>] · dmso · H<sub>2</sub>O and [Ni (bpcam) 2] · H<sub>2</sub>O [Hbpcam = bis (2-pyrimidylcarbonyl) amide], New J. Chem. 41 (14) (2017) 6911–6921.
- [81] Y.Y. Zhu, F. Liu, J.J. Liu, Y.S. Meng, S.D. Jiang, A.L. Barra, W. Wernsdorfer, S. Gao, Slow magnetic relaxation in weak easy-plane anisotropy: the case of a combined magnetic and HFEPR study, Inorg. Chem. 56 (2) (2017) 697–700.
- [82] M. Rathnam, A. Kumar, I. Verma, J. Klak, J. Cano, A.J. Mota, A. Rajput, H. Arora, Discrete unusual mixed-bridged trinuclear Co III 2 Co II and pentanuclear Ni II coordination complexes supported by a phenolate-based ligand: theoretical and experimental magneto-structural study, New J. Chem. 45 (13) (2021) 6053–6066.
- [83] B. Ay, G. Mahmoudi, A. A. Khandar, F.A. Afkhami, A. Toprak, F.I. Zubkov, J. White, J. Kłak, D.A. Safin, A novel paramagnetic coordination polymer, fabricated from Co (NCS) 2 and 2-pyridinecarbaldehyde isonicotinoylhydrazone, Inorg. Chim. Acta 522 (2021) 120335.
- [84] S.Q. Bai, E.Q. Gao, Z. He, C.J. Fang, C.H. Yan, Crystal structures and magnetic behaviour of three new azido-bridged dinuclear cobalt (II) and copper (II) complexes, New J. Chem. 29 (7) (2005) 935–941.
- [85] M.H. Zeng, S. Gao, X.M. Chen, A novel 3D coordination polymer containing pentacoordinate cobalt (II) dimers with antiferromagnetic ordering, Inorg. Chem. Commun. 7 (7) (2004) 864–867.
- [86] S. Youngme, C. Chailuecha, G.A. van Albada, C. Pakawatchai, N. Chaichit, J. Reedijk, Dinuclear triply-bridged copper (II) compounds containing carboxylato bridges and di-2-pyridylamine as a ligand: synthesis, crystal structure, spectroscopic and magnetic properties, Inorg. Chim. Acta 358 (4) (2005) 1068–1078.
- [87] S. Youngme, J. Phatchimkun, N. Wannarit, N. Chaichit, S. Meejoo, G.A. van Albada, J. Reedijk, New ferromagnetic dinuclear triply-bridged copper (II) compounds containing carboxylato bridges: synthesis, X-ray structure and magnetic properties, Polyhedron 27 (1) (2008) 304–318.
- [88] G.A. Seisenbaeva, M. Kritikos, V.G. Kessler, Synthesis, X-ray single crystal and magnetic study of new heteroleptic late transition metal alkoxides with tetranuclear square planar metal core, Co 4Cl<sub>2</sub> (OC<sub>2</sub>H<sub>4</sub>OEt)<sub>6</sub> Co<sub>4</sub>(OMe)<sub>2</sub>(acac)<sub>6</sub> (MeOH)<sub>2</sub> and Zn<sub>4</sub> (OMe)<sub>2</sub>(acac)<sub>6</sub> (C<sub>7</sub>H<sub>8</sub>), Polyhedron 22 (18) (2003) 2581–2586.
- [89] G.A. Seisenbaeva, T. Mallah, V.G. Kessler, Highly symmetric organic ligand-capped Lindqvist structures derived from 3d-elements, Dalton Trans. 39 (33) (2010) 7774–7779.